Computational Fluid Dynamics Modeling of the Effect Of Rotation During Reaming into the Intramedullary Canal of a Long Bone

J. Bahen[1], O. Gaber[1], K. Behdinan[2], J. De Beer[3], P. Zalzal[4] , M. Papini[1] and M. Z. Saghir[1]

Abstract: The penetration of the reamer into the medullary cavity can be compared to a piston entering a cylinder filled with viscous fluid. When the flutes of the reamer are clogged with bone debris, fat and marrow, the piston effect is magnified and larger pressures are usually obtained. This paper considers a reamer with clogged flutes and investigates whether the rotation speed of the reamer has a significant influence on the pressure within the intramedullary cavity. The effect of reamer rotation speed on the pressure distribution within the bone is investigated numerically by solving the full three-dimensional Navier-Stokes equations together with the continuity equation by means of a finite element technique. The model shows that as the rotation speed is increased for a reamer with clogged flutes, the pressure within the intramedullary canal does not exhibit a significant increase.

keyword: Intramedullary reaming, Porous Media, FIDAP computer model, Fat Embolism.

1 Introduction

Over the past 25 years the use of intramedullary nailing for tibial and femoral fractures has become popular, and excellent results for patient recovery have been reported Pell et al. (1993). Unfortunately it has also been observed that intramedullary reaming and nailing of the femur causes the embolization of fat and marrow contents into the venous circulation, causing a condition known as fat embolism syndrome (FES). Large emboli have been observed in the right cavities of the heart within few seconds following reaming Peter et al. (1994). This is believed to be due to the highly elevated pressures caused by the reaming or nailing procedure.

FES is most commonly associated with fractures of long bones of the lower extremity Johnson and Lucas (1996), developing in 0.5% to 2% of all patients with fractures of the long bones, and associated with high morbidity and mortality Pell et al. (1993). Intramedullary pressure elevation during reaming can vary greatly depending on a number of parameters, including the presence or absence of a fracture, the speed of the reamer penetration, and the design of the reamer Peter et al. (1994). Other studies have observed that intramedullary marrow viscosity and the depth of the reamer flutes can have a profound impact on the increased intramedullary pressure Greg and Richard (1997).

The intramedullary canal contains a highly viscous medullary fat. Reaming allows the canal to be open to implant insertion. During this reaming process, however, the cutting flutes can become clogged and congealed, stopping the transportation of debris out of the bone Baumgart et al. (1998). When clogging and congealing of the reamer flutes occurs, penetration of the reamer into the medullary cavity can be compared to a piston entering a cylinder filled with viscous fluid, and the reamer et al displaces a volume of fluid in the cylinder Peter et al. (1994). This can theoretically lead to very high pressure values, as seen with hydraulic instruments Sturmer (1993). As the mean blood pressure in the capillaries is only approximately 25 mmHg, the reaming process can cause the intramedullary pressure to greatly exceed this value at which point fat ejection is inevitable Sturmer (1993). Although the exact pressure when fat ejection occurs is not well established, it is accepted that it will occur due the increased pressure caused by intramedullary reaming, which at times can exceed 1000 mmHg Johnson et al. (1995).

In the literature, numerical attempts to model the fluid flow in bones have been very limited. There are some note worthy exceptions including the work of Orr and Dunne (2000), whose model describes cement flow in the intramedullary cavity. In their work, a simple cylin-

[1] Department of Mechanical and Industrial Engineering, Ryerson University, Toronto, On, Canada

[2] Department of Aerospace Engineering, Ryerson University, Toronto, On, Canada

[3] Henderson Hospital, Hamilton, On, Canada

[4] Mount Sinai Hospital, Toronto, On, Canada

der was first modeled, and later the authors progressed to an actual femoral prosthesis. Their theoretical model was designed to allow the prosthesis bone geometry of an individual patient to be evaluated in terms of probable pressure distributions in the medullary cavity during cemented fixation and in turn to guide the stem design with reference to preparation of the medullary canal. The predicted pressures from their theoretical model were found to be close to those measured experimentally. Gaber (2005) modeled the insertion of a reamer without rotation into the intramedullary canal, using a simple co-axial cylinder model, and were able to closely imitate the behavior of experimental results by Johnson et al. (1995), which used human cadaver femora.

The present study attempts to model intramedullary reaming and insertion with various rotation and insertion rates using the same finite element approach as was used in Gaber (2005).

2   Model Description

Following the work of Gaber (2005), the femur is modeled as two co-axial cylinders with a length of 350mm and an outer diameter of 32 mm. This compares well to the actual model of the femur. See Fig.1 and Fig. 2. The inner diameter of the cylinders is varied from 9 mm to 10 mm, to reflect two differently sized reamers. The lower surface of the inner cylinder is defined in such a way that simulation of the rotation and insertion of the reamer into the bone marrow cavity is possible (see Sect. 3.1.2 for additional details). An important parameter when discussing the causes of FES is bone porosity. The porosity of bone can vary with age and gender and an approximation of this important parameter must be obtained for the simulation. It has been shown Smit et al. (2002) that use of a linear isotropic description of cortical bone as a two level porous medium is an appropriate approximation. Although the average bone porosity ϕ varies in existing studies Smit et al. (2002), Cowin (1999), it can be approximated to 5 %. The permeability κ of bone like the porosity is also quite variable Cowin (1999); an approximate value would be in the range of $3 \times 10^{-9} - 16 \times 10^{-9} \mathrm{m}^2$, Grimm, M.J.; Williams, J.L. (1997). By using the theoretical relationships described in-depth in Smit et al. (2002) poroelastic parameters can also be described for other bone types, by using their experimental data sets.

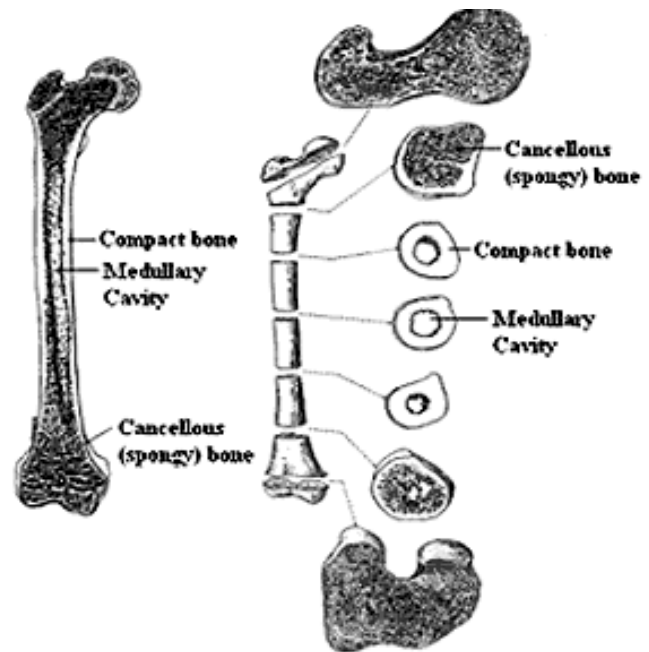Another important input parameter in numerical model-

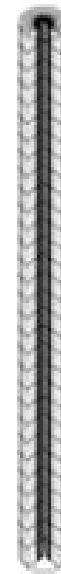**Figure 1** : Femur Profile [Agur, A. (1991)].

Figure 2 : Numerical Model of the Femur.

ing of reaming is the viscosity of the bone marrow. It is known that bovine marrow characteristics greatly resemble those of humans. For this reason, it is commonly used in biomechanical and numerical studies Grimm and Williams (1997). Known values of bovine marrow have

been experimentally calculated to be in the range of 0.04 - 0.4 Pa·s Bryant et al. (1989). It is also known that bone and bone marrow both have similar densities and specific heats. These values are 1810 kg/m^3 and 1256 J/kg K respectively Agar (1991). Biyikli (1986) measured the thermal conductivity of human femora, which ranges from 0.26-0.34 W/(m·K) for fresh specimens, and 0.16 - 0.24 W/(m·K) for dry specimens. The material properties used in this study are summarized in Tab. 1. It should be noted that in our current model the simulation is assumed to be isothermal. This allows the energy equation to be omitted from the calculations, and pressure becomes the dominant force driving the simulation.

3 Governing Equations

3.1 Momentum Equations

The three momentum equations describing laminar, transient, incompressible Newtonian fluid flow through a porous medium can be written using cylindrical components in dimensionless form as follows:

R-Component

$$\frac{Re}{\varphi}\frac{\partial U_r}{\partial \tau} + \frac{1}{Da}U_r = -\frac{\partial P}{\partial R}$$
$$+ \frac{1}{a}\left[\frac{\partial}{R\partial R}\left(\frac{\partial (RU_r)}{\partial R}\right) + \frac{1}{R^2}\frac{\partial^2 U_r}{\partial \theta^2} - \frac{2}{R^2}\frac{\partial U_\theta}{\partial \theta} + \frac{\partial^2 U_r}{\partial Z^2}\right]$$
$$+ Re \tag{1}$$

θ−Component:

$$\frac{Re}{\varphi}\frac{\partial U_\theta}{\partial \tau} + \frac{1}{Da}U_\theta = \frac{1}{R}\frac{\partial P}{\partial \theta}$$
$$+ \frac{1}{a}\left[\frac{\partial}{R\partial R}\left(\frac{\partial (RU_\theta)}{\partial R}\right) + \frac{1}{R^2}\frac{\partial^2 U_\theta}{\partial \theta^2} + \frac{2}{R^2}\frac{\partial U_r}{\partial \theta} + \frac{\partial^2 U_\theta}{\partial Z^2}\right] \tag{2}$$

Z-Component

$$\frac{Re}{\varphi}\frac{\partial U_Z}{\partial \tau} + \frac{1}{Da}U_Z = \frac{\partial P}{\partial Z}$$
$$+ \frac{1}{a}\left[\frac{1}{R}\frac{\partial}{\partial R}\left(\frac{R\partial U_Z}{\partial R}\right) + \frac{1}{R^2}\frac{\partial^2 U_Z}{\partial \theta^2} + \frac{\partial^2 U_Z}{\partial Z^2}\right] \tag{3}$$

The dimensionless variables used to obtain the above equations are as follows:

$$R = \frac{r}{L}, \quad Z = \frac{z}{L}, \quad U_r = \frac{u_r}{u_0}, \quad \tau = \frac{tu_0}{L}, \quad U_\theta = \frac{U_\theta}{u_0},$$
$$U_Z = \frac{U_Z}{u_0}, \quad P = \frac{pL}{\mu u_0}, \quad Re = \frac{\rho u_0 L}{\mu}, \quad a = \frac{\mu}{\bar{\mu}},$$
$$Da = \frac{\kappa}{L^2}, \quad u_0 = \sqrt{g \times L} \tag{4}$$

where r is the bone radius, L is the characteristic length of the cylindrical bone representation, u_0 is the characteristic velocity adopted in the non-dimensionalization, t is the time in seconds, ρ is the density in kg/m^3 and κ is the bone permeability in m^2. Eq.1 to Eq.3 describe the Momentum (Navier-Stokes) equation for the fluid flow in a porous medium, where Re is Reynolds number and Da is Darcy number. U_R, U_θ and U_Z represent the dimensionless fluid velocity in the radial (R), angular (θ) and axial (Z) direction, respectively. Finally, μ and p represent the viscosity and the pressure, respectively. The non dimensional variable a is defined as the ratio of the fluid viscosity to the effective viscosity. The effective viscosity $\bar{\mu}$ is the viscosity value that is used as an input during the simulation in conjunction with the coefficient a. It is two orders of magnitude less than μ and aids in the computational simulation.

3.1.1 Continuity Equation

In numerical modeling, the continuity equation, Eq. 5, must also be satisfied.

$$\frac{1}{R}\frac{\partial}{\partial R}(RU_r) + \frac{1}{R}\frac{\partial U_\theta}{\partial \theta} + \frac{\partial U_z}{\partial Z} = 0 \tag{5}$$

3.1.2 Boundary Conditions

The predictions of the present model will be compared to the results of Johnson et al. (1995), who monitored the pressure distribution within a femur during intramedullary reaming, and Gaber (2005) who used a numerical model to simulate the experiment without rotation of the reamer. In the experiments of Johnson et al. (1995) a frozen cadaveric femur was cleaned of all flesh, and instrumented with pressure taps mounted at mid-shaft. Prior to power reaming there was initial canal broaching with an awl, and guide wire placement. Power reaming then began with a 9 mm reamer which produced the initial cavity. The reaming speed was 2.58 cm/s ($\pm$0.6 cm/s). Since there was no living tissue surrounding the bone, the cavity stayed empty after the initial ream. In

Table 1 : Physical Properties

Physical properties of Compact Bone section		Physical properties of Medullary section	
Symbol	Value	Symbol	Value
ϕ	0.05	ϕ	0.95
κ	$3 \times 10^{-9} - 16 \times 10^{-9} \text{m}^2$	κ	$3 \times 10^{-7} - 16 \times 10^{-7} \text{m}^2$
ρ	1810 kg/m^3	ρ	1810 kg/m^3

reality, the cavity would fill up with blood and fat instantaneously. This was simulated by refilling the bone cavity with Albumin. The second reaming was done using a 10mm reamer. Pressure values at the mid-point were obtained for both reaming cases and were plotted against the experimental results.

As anticipated, the boundary conditions used in the present model are chosen to simulate the experiments performed by Johnson et al. (1995) and the simulation performed by Gaber (2005). It is worth noting that in Johnson et al. (1995) Teflon was wrapped around the bone to prevent escape of intramedullary canal contents, and to maintain a constant temperature of $37\,°C$ (thus maintaining our assumption that the process is isothermal, and that the energy equation can be omitted for the sake of simplicity). The boundary conditions adopted in our model are:

Velocity specified as zero at the lateral surface of the outer cylinder, as well as at the top and bottom of the outer cylinder and the top of the inner cylinder. Therefore, no fluid can escape through the side walls or the top and bottom of both cylinders. The velocity boundary conditions at r = 1.6 cm and at z = 0 and 35 cm therefore are :

$$U_r = 0, \quad U_\theta = 0, \quad U_Z = 0 \tag{6}$$

In practice, at the tip of the inner cylinder, the surface velocity is set to be equal to the insertion rate to mimic the movement of the reamer as it advances at a constant velocity.

$$U_Z = \text{insertion velocity} \tag{7}$$

The lower part of the inner cylinder surface is also given a boundary conditions to imitate the rotation of the reamer.

$$U_\theta = \text{Rotation speed} \tag{8}$$

4   Solution Technique

The non-linear equations Eq.1 to Eq.3 and Eq.5 were solved simultaneously using the segregate solver. An eight nodes hexahedral element was used for this simulation, where four unknowns, radial velocity, angular velocity, axial velocity and pressure were evaluated at each element, as shown in Fig. 1. When setting up the problem, care was provided when specifying the allowable errors for the solution convergence. Too large allowance would result in false convergence, and too small would result in either a very lengthy calculation time, or no convergence at all. The two main error parameters that the finite element program takes into consideration are the velocity convergence tolerance, and the residual vector convergence tolerance. The velocity convergence tolerance is defined by the equation:

$$\left\| \frac{\zeta_i - \zeta_{i-1}}{\zeta_i} \right\| \leq \zeta_{error} \tag{9}$$

where ζ is the solution velocity vector. The error for this case was specified as 1×10^{-3}. The residual error on the other hand is defined as:

$$\left\| \frac{R_i}{R_0} \right\| \leq R_{error} \tag{10}$$

The error for this case was also specified to be 1×10^{-3}. The norm $\|\|$ is a root mean square norm.
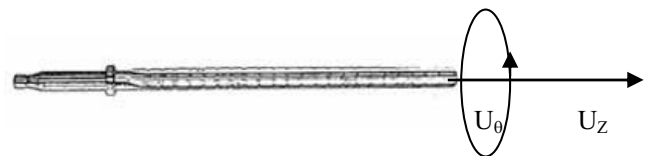

Figure 3 : Reamer with Velocity Boundary Conditions

5   Mesh Sensitivity

To ensure the correctness of the model, mesh sensitivity was considered to reduce the number of elements and nodes in the mesh while maintaining accurate results. This is usually done to minimize computational time and memory, while keeping the model accurate.

Gaber (2005) provided a grid refinement study for the number of axial nodes in the model. However, due to the present additional boundary conditions and their direct effect on the nodes on the inner cylinder edge, refined mesh sensitivity has been performed also for these radial nodes. A non-uniform boundary layer grid structure starting at the edge of the inner cylinder has been applied. A large aspect ratio for the node location starting from the edge of the inner cylinder has been initially chosen. This aspect ratio has been gradually decreased until the optimum mesh was found. Due to the transient nature of the experiment the average pressure taken at 3 different times 0.68 s, 3.39 s and 6.80 s (which represents the initial, middle and final time steps) has been considered as a key parameter for the refinement study.

As the aspect ratio has been decreased, the error value has been computed. When the percentage error of the average pressure values between successively finer meshes was less than 5%, the second last mesh was deemed adequate. In our case using an initial distance of 5% of the inner radius the optimum aspect ratio for the radial mesh is 1.4.

6   Results

Fig. 1 shows the location of the compact bone layer as well as the intramedullary section in the femur. The inner diameter of the cylinder is used to mimic the intramedullary section of the bone and is adjusted for each reamer size to make a tight sealed fit. An azimuthal velocity is imposed on the lower surface of the inner cylinder to simulate the rotation of the reamer during insertion. As anticipated, the cadaveric femur bone used in Johnson et al. (1995) was wrapped in Teflon so that no fluid was allowed to escape through the pores of the bone, a condition reflected in the choice of the zero velocity boundary condition on the outer surface of the cylinder. Two cases are solved, to compare to both Johnson et al. (1995) and Gaber (2005). The first case is introduced to examine the effect of an insertion of 9mm reamer, and the second case an insertion of a 10mm reamer.

6.1   Case 1: Insertion with 9mm Reamer

The first reamer size that Johnson et al. (1995) used was the 9mm reamer. Pressure values were recorded at the mid-shaft as the reamer was inserted into the bone. Gaber (2005) investigated the effect of insertion without rotation and his results are depicted in the Fig. 4 and Fig. 8 as 0 rpm values. For the present simulation rotational speeds ranging from 1 rpm to 450 rpm are chosen. These values are used to simulate actual rotational speeds evident during orthopedic procedures. Mousavi et al. (2001), Mousavi et al. (2002), in fact, investigated intramedullary pressures in sheep during reaming and reported rotational speeds of 150 rpm and 450 rpm. In the present simulation 450 rpm is taken as the high rotational speed and 100 rpm as the low speed. 1 rpm has been used simply to ensure the model was operating properly. With the 9mm reaming case two scenarios are analyzed, the case of varying viscosity and the case of different insertion rates.

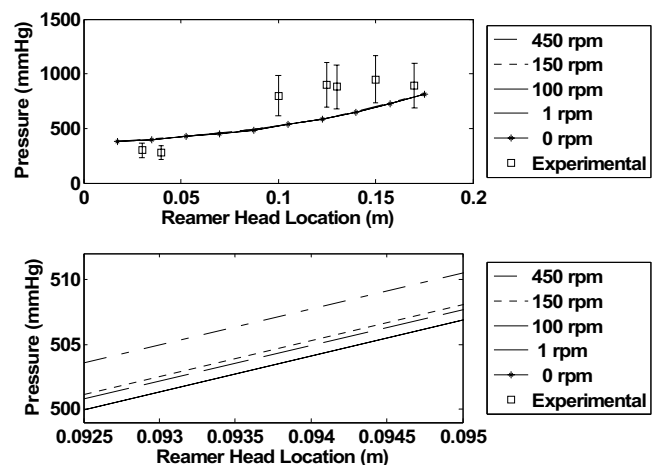#### 6.1.1   Varying Insertion Rate

Figure 4 : Percentage Increase in Intramedullary Pressure at the Mid-shaft of 100 rpm over 0 rpm for 9 mm 2.58 cm/s insertion: (a) Full View Bottom (b) Magnified View

In Fig. 4 (a) and 4 (b) the variation of pressures over the reamer location is presented for an insertion speed of 2.58 cm/s. In this case the viscosity of the marrow is assumed to be equal to $\mu = 0.22$ Pa·s. As is evident in this simulation as well as in Gaber (2005), when the reamer
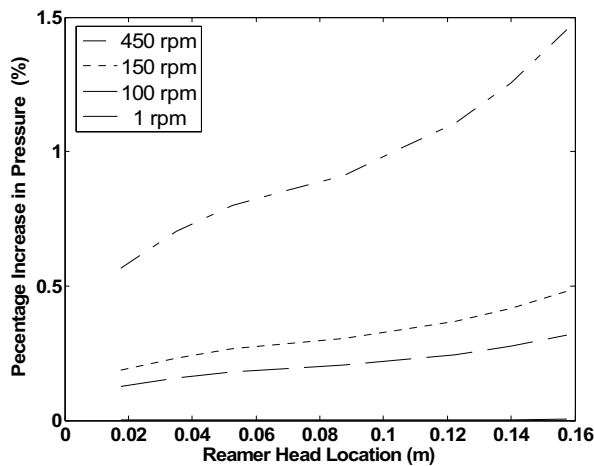
Figure 5 : Percentage Increase in Pressure due to the Added Rotation with a 9 mm Reamer with 2.58 cm/s Insertion
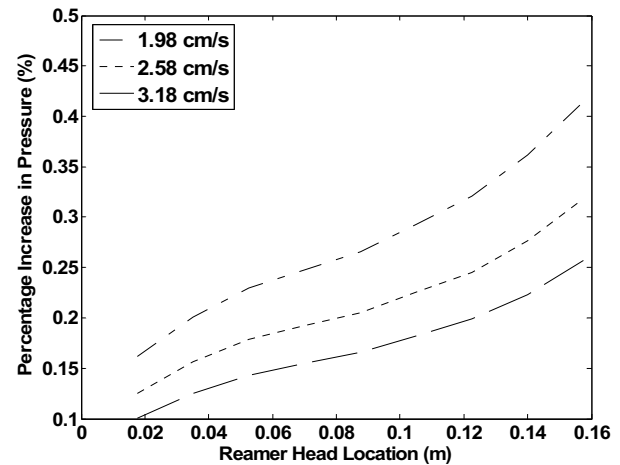

Figure 6 : Percentage Increase in Pressure of 100 rpm due to Varying Insertion Rates

Figure 7 : Percentage Pressure Increase of 100 rpm due to Varying Viscosity

advances the pressure increases continuously in an exponential fashion, and compares well with the experimental results.

Looking at Fig. 4(b) we can see more clearly the small impact the rotational component has on the overall pressure distribution. This shows that once the flutes are clogged the speed of the rotation does not affect the pressure increase because no bone and marrow debris are being transported out of the bone. Fig. 5 displays the exact pressure increases due to the added rotational energy. Clearly the rotational component has little effect as all pressure increases are less than 1%.

The mean rate of insertion was given as 2.58 ($\pm$ 0.6) cm/s in Johnson et al. (1995). In the attempt to determine whether rotation would have any effect at the minimum and maximum extremes of the insertion, other simulations have been carried out for 1.98 cm/s and 3.18 cm/s. The base line comparison is made to Gaber (2005) whose results are the control 0 rpm. Although Fig. 6 shows larger percentage increases for the slower insertion rates all values are in the range of less than 1 % and can be regarded as insignificant with respect to the overall pressure increase.

6.1.2 Varying Viscosity

The present model is based on the same assumptions of Gaber (2005), i.e., that back flow fluid is not allowed to escape from the interface between the bone and reamer,
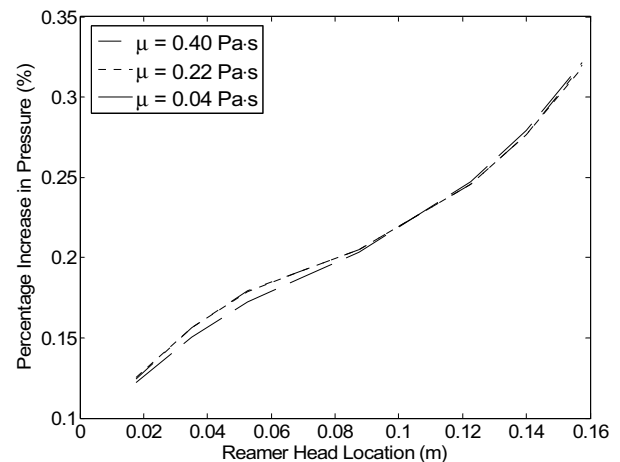
which is an idealized condition. Nevertheless, it should be noted that Johnson et al. (1995) did not report any fluid escaping. To mimic the results of Gaber (2005) the simulation have been repeated with the initial insertion rate of 2.58 cm/s and varying viscosities to examine the effect of rotation with different viscosities.

The results of Gaber (2005) showed significant changes in intramedullary canal pressure at the mid-shaft during insertion, and found that the marrow viscosity played an important role in determining the pressure variation as a function of the insertion rate. In our study, it is found that the effect of the rotation is minimal regardless of the viscosity value, as is shown in Fig. 7, which displays the
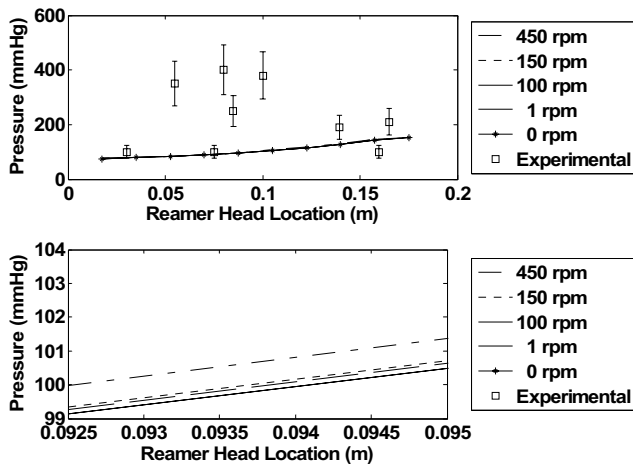
Figure 8 : Pressure Variation during Insertion of a 10 mm Reamer at a Constant Velocity of 2.58 cm/s Top (a) Full View Bottom (b) Magnified View
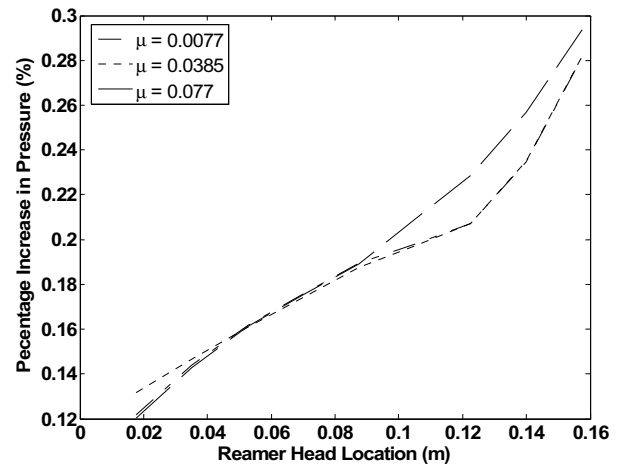

Figure 9 : Percentage Increase in Intramedullary Pressure at the Mid-Shaft of 100 rpm during insertion of 10mm Reamer with Varying Viscosities

percentage increase of intramedullary canal pressure at the mid-shaft with 100 rpm over 0 rpm at varying viscosities. Apparently, the added rotation is not fulfilling its purpose of extracting the debris at a faster rate because the flutes are clogged; and with the rotational speeds used in the reaming procedure an insignificant amount of energy is added to elevate the intramedullary pressure.

6.2 Case 2: Insertion with 10mm Reamer

In the experiments of Johnson et al. (1995) the same bone that was used in the initial reaming using the 9mm reamer was subsequently used for the reaming using the 10mm reamer. As explained before, to simulate the refilling of the reamed portion of the intramedullary canal with blood and marrow the bone was filled with albumin before reaming the bone again using the 10mm reamer. In Johnson et al. (1995) there is no mention of the specific type of albumin; hence there is an uncertainty about the viscosity values to be used in the simulation. Gaber (2005) used varying viscosity values of albumin between 0.0077 Pa·s and 0.077 Pa·s. Our analysis uses these values.

6.2.1 Alternative Reamer Diameter

Using the new viscosity values the simulation has been repeated using the 10mm reamer with an insertion rate of 2.58 cm/s, with varying rotation rates to determine if the rotational speed has an impact on different diam-

eter reamers. As for the case for the 9mm reamer we again see for the 10mm reamer the minimal effect that the rotation of the reamer has on the distribution of the intramedullary pressure. Fig. 8(a) and 8(b) display the intramedullary canal pressure at mid-shaft with viscosity equal to μ=0.0385 Pa·s.

6.2.2 Varying Viscosity

The viscosity of albumin over a range of values has been used to understand the effect of changing viscosities with different reamer diameters. The viscosity has been varied from 0.0077 Pa·s and 0.077 Pa·s. What is evident after the simulations is that the rotation rate has little effect on the overall intramedullary pressure build-up. Fig. 9 shows this insignificant effect very clearly (1%).

7 Conclusion

When reaming of the long bones is conducted it is known that the flutes of the reamer become clogged with debris and the reaming procedure becomes similar to that of a hydraulic piston in a cylinder filled with viscous fluid Sturmer (1993). From our analysis we can see that when this occurs the pressure increase in the intramedullary cavity is unaffected by the rotation rate of the reamer. This has been shown to be true regardless of the insertion speed or viscosity of the marrow. The clinical implications for orthopedic surgeons performing the range of surgical procedures detailed in the introduction, is that,

based on our findings the surgeon need not to be concerned with the reamer rotation rate if the flutes of the reamer have become clogged, as this will have a minimal effect on intramedullary pressure.

It should be noted that although the rotation rate of the reamer has been found to have no significant effect on the pressure increase in the intramedullary cavity, it is possible that the rotation rate affects the temperature increase of the bone tissue during reaming. This temperature change due to reaming is a topic requiring further investigation, as it has been shown that if the reaming temperature exceeds 44.1 °C, cell enzymes are damaged and the bone healing process is negatively influenced Muller et al. (1993).

Nomenclature

a	: Darcy coefficient	[-]
Da	: Darcy number	[-]
L	: Reference length	[m]
p	: Pressure	[Pa]
P	: Dimensionless pressure	[-]
r	: Radial direction	[m]
R	: Dimensionless radial direction	[m]
Re	: Reynolds number	[-]
t	: Time	[s]
u_r	: Velocity in the r direction	[m/s]
U_r	: Dimensionless velocity in the r direction	[-]
u_θ	: Velocity in the θ direction	[m/s]
U_θ	: Dimensionless velocity in the θ direction	[-]
u_z	: Velocity in the z direction	[m/s]
U_z	: Dimensionless velocity in the z direction	[-]
u_0	: Reference velocity in axial direction	[m/s]
Z	: Dimensionless axial direction	[-]

Greek symbols

ζ	: Velocity convergence tolerance	[-]
κ	: Permeability	[m^2]
μ	: Viscosity	[Pa·s]
$\bar{\mu}$	: Effective Viscosity	[Pa·s]
ρ	: Density	[kg/m^3]
φ	: Porosity	[-]

References

Agur, A. (1991): Grant's Atlas of Anatomy, 9th edition. Williams and Wilkins, Philadelphia, 1991.

Baumgart,F.; Kothler, G.; Ochsner P.E. (1998): The Physics of Heat Generation During Reaming of the Medullary Cavity, *Injury*, vol. 29, Supplement 2, pp. S11-S25.

Biyikli, S. (1986): Measurements of Thermal Properties for Human Femora. Journal of Biomedical Materials Research. Vol. 20, pp. 1335-1345.

Bryant, J.D.; David, T.; Gaskell, P.H.; King, S.; Lond, G. (1989): Rheology of Bovine Bone Marrow. *Proc. Instn Mech. Engrs*, vol. 203, pp. 71-75.

Cowin, S.C. (1999): Bone Poroelasticity, *Journal of Biomechanics*, vol. 32, pp. 217-238.

Gaber, O. (2005) MASc. Thesis, *Ryerson University*.

Greg, A.; Richard, F.K. (1997): Biofluid Mechanics of Intramedullary Reaming. *Bioengineering Conference*, vol.35, pp. 581-582.

Grimm, M.J.; Williams, J.L. (1997): Measurements of Permeability in Human Calcaneal Trabecular Bone. *Journal of Biomechanics*, vol. 30, pp. 743-745.

Johnson, J.A.; Berkshire, A.; Leighton, R.K.; Gross, M.; Chess, D.G.; Petrie, D. (1995): Some Basic biomechanical characteristics of medullary pressure generation during reaming of the femur. *Injury*, vol. 26, pp. 451-454.

Johnson, M.J.; Lucas, G.L. (1996): Fat Embolism Syndrome. *Orthopedics,* vol.19. pp. 41-49.

Mousavi, M.; Kolonja, A.; Schaden, E.; Giibler, C.; Etheshami, J.R.; Vecsei, V. (2001): Intracranial pressure-alterations during controlled intramedullary reaming of femoral fractures: an animal study. *Injury*, vol. 32, pp. 679-682.

Mousavi, M.; Davis, R.; Schwendenwein, I.; Schaden, E.; Marlovits, S.; Kolonja, A.; Schwanzer E.; Heinz T.; Vecsei, V. (2002): Influence of Controlled Reaming on Fat Intravasation after femoral Osteotomy in Sheep. *Clinical Orthopedics and Related Research*, vol. 394, pp. 263-370.

Muller, C.; McIff, T.; Rahn, BA.; Pfister, U.; Weller, S. (1993): Intramedullary pressure, strain on the diaphysis and increase in cortical temperature when reaming the femoral medullary cavity-a comparison of blunt and

sharp reamers. *Injury*, vol. 24, Supplement 3, pp. S22-S30.

Orr, J.F.; Dunne, N.J. (2000): Development of a Computer Model to Predict Pressure Generation Around Hip Replacement Stems. *Proceedings of the Institution of Mechanical Engineers Part H*, vol. 214, pp. 645-658.

Pell, A.; Christie, J.; Keating, J.; Sutherland, G. (1993): The Detection of Fat Embolism By Trasoesophageal Echocardiography During Reamed Intramedullary Nailing. *The Journal of Bone and Joint Surgery*, vol. 75-B, pp.921-925.

Peter, R.R.; Selz, T.; Koestli, A. (1994): Influence of the Reamer Shape on Intraosseus Pressure during Closed Intramedullary Nailing of the Unbroken Femur. *Injury*, vol. 24, Supplement 3, pp.S48-S55.

Smit, T.H.; Huyge, J.M.; Cowin, S.C. (2002): Estimation of the Poroelastic Parameters of Cortical Bone. *Journal of Biomechanics*, vol. 35, pp. 829-835 .

Sturmer, K. M. (1993): Measurement of Intramedullary Pressure in an Animal Experiment and Proposition to Reduce the Pressure Increase. *Injury*, vol. 24, Supplement 3, pp. S7-21.